



HAL
open science

A simple analytical model to study and control azimuthal instabilities in annular combustion chambers

Jean-François Parmentier, Pablo Salas, Pierre Wolf, Gabriel Staffelbach,
Franck Nicoud, Thierry Poinsot

► **To cite this version:**

Jean-François Parmentier, Pablo Salas, Pierre Wolf, Gabriel Staffelbach, Franck Nicoud, et al.. A simple analytical model to study and control azimuthal instabilities in annular combustion chambers. *Combustion and Flame*, 2012, 159 (7), pp.2374-2387. 10.1016/j.combustflame.2012.02.007 . hal-00802059

HAL Id: hal-00802059

<https://hal.science/hal-00802059>

Submitted on 18 Mar 2013

HAL is a multi-disciplinary open access archive for the deposit and dissemination of scientific research documents, whether they are published or not. The documents may come from teaching and research institutions in France or abroad, or from public or private research centers.

L'archive ouverte pluridisciplinaire **HAL**, est destinée au dépôt et à la diffusion de documents scientifiques de niveau recherche, publiés ou non, émanant des établissements d'enseignement et de recherche français ou étrangers, des laboratoires publics ou privés.

A simple analytical model to study and control azimuthal instabilities in annular combustion chambers

J.-F. Parmentier^a, P. Salas^b, P. Wolf^a, G. Staffelbach^a, F. Nicoud^c, T. Poinsot^d

^a*CERFACS, CFD team, 42 Av Coriolis, 31057 Toulouse, France*

^b*INRIA Bordeaux - Sud Ouest, HiePACS Project, joint INRIA-CERFACS lab. on High Performance Computing*

^c*Université de Montpellier 2. I3M.UMR CNRS 5149*

^d*IMF Toulouse, INP de Toulouse and CNRS, 31400 Toulouse, France*

Abstract

This study describes a simple analytical method to compute the azimuthal modes appearing in annular combustion chambers and help analyzing experimental, acoustic and LES (Large Eddy Simulation) data obtained in these combustion chambers. It is based on a one-dimensional zero Mach number formulation where N burners are connected to a single annular chamber. A manipulation of the corresponding acoustic equations in this configuration leads to a simple dispersion relation which can be solved by hand when the interaction indices of the flame transfer function are small and numerically when they are not. This simple tool is applied to multiple cases: (1) a single burner connected to an annular chamber ($N = 1$), (2) two burners connected to the chamber ($N = 2$), (3) four burners ($N = 4$). In this case, the tool also allows to study passive control methods where two different types of burners are mixed to control the azimuthal mode. Finally, a complete helicopter chamber ($N = 15$) is studied. For all cases, the analytical results are compared to the predictions of a full three-dimensional Helmholtz solver and a very good agreement is found. These results show that building very simple analytical tools to study azimuthal modes in annular chambers is an interesting path to control them.

Keywords: azimuthal modes, analytical, combustion instabilities

1. Introduction

Azimuthal modes are combustion instabilities which appear in annular chambers of many gas turbines. These modes are powerful and can lead to vibrations and structural damage [1, 2, 3]. They should be eliminated at the design stage, something which is difficult today because fundamental issues in terms of mechanisms and modeling are not mastered yet.

The first question is to know why these modes appear by studying their linear stability characteristics. Most models used to predict stability in annular chambers are based on one-dimensional network views of the chamber [4, 5, 2] in which each burner is only influenced by the flow rate fluctuation it is submitted to by the azimuthal acoustic mode. In most of these models all burners are supposed to be independent from their neighbours and to have the same transfer function (ie the same relation between inlet burner velocity variations u' and total heat release rate fluctuations q'). This assumption has been checked in one case corresponding to an annular helicopter chamber using LES [6] but this may not be true in general: in liquid-fueled rocket engines or more generally in burners containing multiple jets [7], the interaction between neighbouring flames can lead to instability and transverse modes. This may happen in gas turbines too and require other modeling approaches than the existing ones.

Even if burners can be assumed to respond in a one-dimensional manner to acoustic perturbations, determining their flame response (usually measured as a Flame Transfer Function) remains a challenge [8, 9, 10]. FTFs are the key elements of the majority of acoustic solvers for combustion stability. At some point, these solvers need to characterize the flame response to the acoustic field [11, 12] and the FTF is the most common solution. The problem is that FTFs depend on multiple parameters (regime but also pulsation amplitude, wall temperature, pilot flames, etc) so that an accurate description of FTF is often not available [13, 14]. A second difficulty is to exploit FTF in an acoustic code taking into account the complexity of the geometry [15, 16]. When such simulations are performed, another difficulty linked to the structure of these modes arises [17]: in annular combustion chambers, the first (and sometimes second) azimuthal acoustic mode is often the strongest mode [18, 1, 19]. Azimuthal modes can appear as standing wave modes or rotating modes and both are observed in gas turbines. Bifurcations between standing and turning modes may be due to non-linear effects: Schuermans et al. [2, 19] propose a non-linear theoretical approach showing that standing

wave modes can be found at low oscillation amplitudes but that only one rotating mode is found for large amplitude limit cycles. Other explanations can be found in linear approaches: standing modes would appear only in perfectly axisymmetric configurations while any symmetry modification would lead to rotating modes [20, 21].

Using experiments to study these issues is difficult because multiburner combustion chamber rigs are expensive and rare. An elegant solution is the azimuthal Rijke tubes system [22] where flames are replaced by electric heaters even though some of the physics of real flames is probably lost. A new approach is now possible using massively parallel computations and Large Eddy Simulation (LES) [23, 24, 25]. Such LES solvers can predict instabilities in a reacting flow configuration [12, 26] but their cost for full annular chambers [6, 27] remains prohibitive. Moreover, these simulations can not be repeated easily and can not be used to optimize chamber designs to control azimuthal modes.

Independently of the exact structure of these modes, gas turbine experts are mostly interested in avoiding them or controlling them. This usually requires expensive tests, mainly because guidelines to look for a stable configuration are often missing. Of course, fully active combustion instability control [28, 29] would also be a solution and it has been successfully tested on certain industrial gas turbines (Siemens for example). However, the cost of active control and its difficult certification for aero engines make it less attractive today than trying to understand azimuthal modes and building combustors which are intrinsically stable. To reach this goal, both experiments and simulations are too long and do not provide enough insight into the sources of the coupling. In addition to simulation and experiments, simple analytical models able to analyze the basic nature of azimuthal modes would be very useful. The recent work of Moeck et al. [22] shows how theoretical models can be used to understand azimuthal modes in a model annular combustor where flames are replaced by electrical heaters. The present paper describes an analytical approach for azimuthal instability modes in annular chambers which is even simpler than the method described in [22], but captures enough of the physics of these instabilities to understand modes observed experimentally and numerically and to analyze methods to control these modes.

The model described here is based on a network view of annular chambers [30, 31, 32]: it describes all acoustic waves as one-dimensional waves propagating in an annular chamber fed by burners (Fig. 1). The analysis works

for any number of burners connected to an annular chamber even though the corresponding mathematics become more complex. The effects of flames are described using a simple flame transfer function in each burner. While some previous works take into account acoustic coupling between plenum and combustion chamber [33], this is not the case in this model where burners have a closed end at the upstream end. Moreover only purely azimuthal modes are considered.

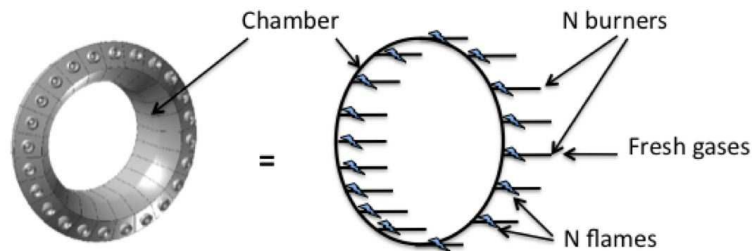


Figure 1: Simplification of annular gas turbine geometry for acoustic model.

The analytical formulation is described in Section 2. Applications are then presented for different configurations, starting from the simplest one ($N = 1$: a single burner connected to an annular chamber, Section 5), then using the model for $N = 2$ (Section 6) and 4 (Section 7). For each case, the frequencies and the structure of the modes are discussed. Results are compared to a 3D Helmholtz solver [16] in an academic geometry. Stability maps are obtained in terms of FTF delay τ for all modes. Two different types of burners are combined (this is usually obtained by a small geometrical modification of the swirler geometry on certain burners while keeping the others the same) to predict how such changes modify the modes and their growth rates, suggesting that certain locations of the modified burners are more efficient than others. This simple analytical formulation provides useful guidelines to understand experimental or numerical results. Finally the model is tested in 3D complex geometry corresponding to a full annular reverse flow helicopter combustion chamber composed of 15 burners (Section 8). Results are compared to those obtained with the a 3D Helmholtz solver in term of stability map.

2. Mathematical description

2.1. Case description

The model is based on a network view of the annular chamber fed by burners (Fig. 1). Only azimuthal modes of the chamber are considered. These modes correspond to longitudinal modes of the burners. The gas dynamics is described using the standard linearized acoustics for perfect gases in the low Mach number approximation. Mean density and sound speed in the annular chamber are noted ρ^0 and c^0 respectively. The flames are supposed to be located at the burners extremity ($z_{f,i} \simeq l_i$, see Fig. 2) so that all burners are assumed to be at the same mean temperature, with a mean density and sound speed noted ρ_u^0 and c_u^0 respectively (subscript u stands for unburnt gases). The perimeter and the section of the annular chamber are noted $2L$ and S respectively. The length and the section of a burner are noted l_i and s_i , where the subscript i is used to designate a particular burner. All numerical applications will correspond to an industrial gas turbine whose characteristics are defined in Table 1.

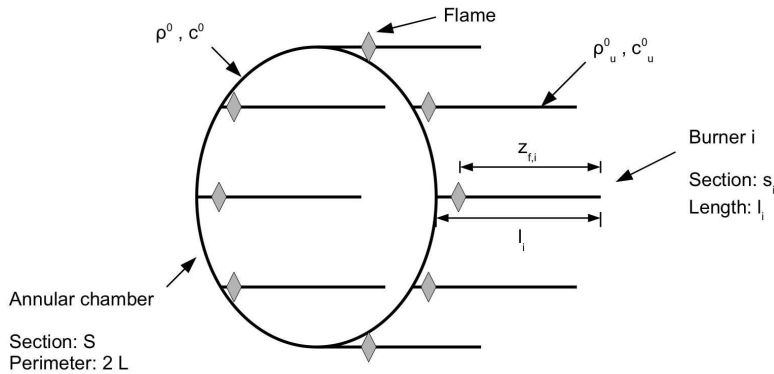


Figure 2: Network representation of the chamber and burners.

2.2. Flow description

The chamber is decomposed into N tubes of length d_i , where d_i is the distance between burners $i - 1$ and i (Fig. 3). Values of d_i are linked to L by $\sum d_i = 2L$ where L is the half-perimeter of the annular chamber.

Chamber			
Half perimeter	L	6.59	m
Section	S	0.6	m^2
Burners			
Lengths	l	0.55	m
Sections	s	0.03	m^2
Fresh gases			
Mean pressure	p^0	$2 \cdot 10^6$	Pa
Mean temperature	T_u^0	700	K
Mean density	ρ_u^0	9.79	kg/m^3
Mean sound speed	c_u^0	743	m/s
Burnt gases			
Mean pressure	p^0	$2 \cdot 10^6$	Pa
Mean temperature	T^0	1800	K
Mean density	ρ^0	3.81	kg/m^3
Mean sound speed	c^0	1191	m/s
Flame parameters			
Interaction index	n	1.57	

Table 1: Parameters used for numerical applications. They correspond to a large scale industrial gas turbine.

Under the linearized acoustics assumptions, the pressure and velocity fluctuations inside part i of the chamber can be written as:

$$p'_i(x, t) = (A_i \cos(kx) + B_i \sin(kx)) e^{-j\omega t} \quad (1)$$

$$\rho_u^0 c_u^0 u'_i(x, t) = j (A_i \sin(kx) - B_i \cos(kx)) e^{-j\omega t} \quad (2)$$

where $j^2 = -1$, $k = \omega/c^0$ is the wavenumber and A_i and B_i are complex constants to determine using boundary conditions. The coordinate x takes its origin at burner $i - 1$. Under the same hypothesis, the pressure and velocity fluctuations inside each burner i can be written as:

$$p'_{u,i}(z, t) = (A_{u,i} \cos(k_u z) + B_{u,i} \sin(k_u z)) e^{-j\omega t} \quad (3)$$

$$\rho_u^0 c_u^0 w'_i(z, t) = j (A_{u,i} \sin(k_u z) - B_{u,i} \cos(k_u z)) e^{-j\omega t} \quad (4)$$

with $k_u = \omega/c_u^0$ and $A_{u,i}$ and $B_{u,i}$ are two complex constants. The total numbers of unknowns of the problem is equal to $4N$: the amplitudes A_i, B_i ($2N$) and $A_{u,i}, B_{u,i}$ ($2N$).

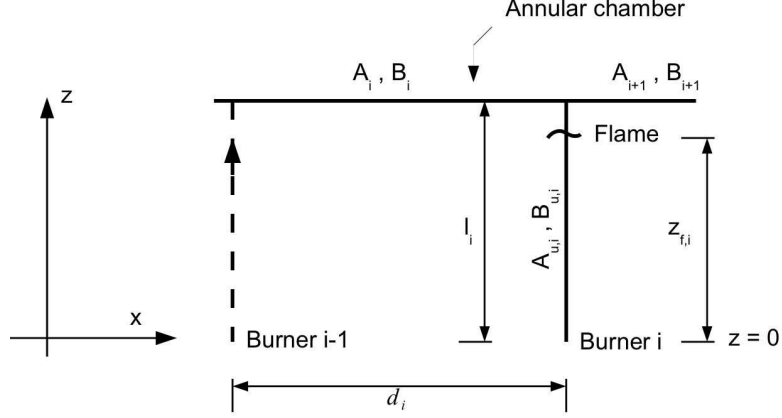


Figure 3: Decomposition of the chamber into N tubes.

Flames in the burner are assumed to be planar and compact: their thickness is negligible compared to the acoustic wave-length. At low mach number, jump conditions through the flames imply equality of pressure and an extra volume source term due to unsteady combustion [12]:

$$p'_{u,i}(z_{f,i}^+, t) = p'_{u,i}(z_{f,i}^-, t) \quad (5)$$

$$s_i w'_i(z_{f,i}^+, t) = s_i w'_i(z_{f,i}^-, t) + \frac{\gamma_u - 1}{\gamma_u p^0} \dot{\Omega}'_{T,i} \quad (6)$$

where $z_{f,i}$ is distance between the beginning of the burner i and the location of the flame i , p^0 is the mean pressure and γ_u is the heat capacity ratio of fresh gases. The unsteady heat release $\dot{\Omega}'_{T,i}$ is expressed in terms of the velocity using a $n - \tau$ model [34]:

$$\frac{\gamma_u - 1}{\gamma_u p^0} \dot{\Omega}'_{T,i} = s_i n_i e^{j\omega\tau_i} w'_i(z_{f,i}^-, t) \quad (7)$$

where the interaction index n_i and the delay τ_i are input data describing the interaction of the flame i with acoustics. Moreover, the flames are assumed to be located at the burners extremity ($z_{f,i} = l_i$).

2.3. Boundary conditions

The inlets of the burners ($z = 0$ in Fig. 3) are considered as walls, leading to zero velocity fluctuations:

$$w'_i(z = 0, t) = 0 \quad (8)$$

The intersection of the burners with the chamber at $z = l_i$ is a 'T' configuration. The jump condition at the 'T' intersection requires equal pressure on each sides of the tubes as well as conserved unsteady volume flow rate [12]. With the flame located at the burner extremity, the combination of these boundary conditions with the flame jump conditions (Eqs. (5), (6) and (7)) leads to:

$$p'_i(x = d_i) = p'_{i+1}(x = 0) \quad (9)$$

$$p'_{u,i}(z = l_i) = p'_{i+1}(x = 0) \quad (10)$$

$$S u'_{i+1}(x = 0) = S u'_i(x = d_i) + s_i w'_i(z = l_i) (1 + n_i e^{j\omega\tau_i}) \quad (11)$$

where the fluid velocity in the burner $w'_i(z = l_i)$ is taken just before the flame ($w'_i(z = l_i) = w'_i(z = z_{f,i}^-)$).

These boundary conditions can be expressed as a function of the waves amplitudes A_i , B_i , $A_{u,i}$ and $B_{u,i}$, leading to a set of $4N$ linear equations (N wall conditions and 3 at each 'T' intersections). The linear system given by $4N$ unknowns with $4N$ linear equations gives non-null solutions if and only if its determinant is null. This dispersion relation can be obtained by calculating the determinant of the $4N \times 4N$ matrix describing the configuration. However the expression of this matrix is not trivial. The next section presents a methodology to reduce the problem to the calculation of the determinant of a 2×2 matrix enabling a simple explicit calculation of the eigenfrequencies and mode structures for any number of burners.

3. Eigenfrequencies calculation

3.1. Transfer matrix

The wall condition at the beginning ($z = 0$) of each burner (Eq. (8)) enables us to express pressure and velocity fluctuations in the burner i as:

$$p'_{u,i}(z, t) = A_{u,i} \cos(k_u z) e^{-j\omega t} \quad (12)$$

$$\rho_u^0 c_u^0 w'_i(z, t) = j A_{u,i} \sin(k_u z) e^{-j\omega t} \quad (13)$$

Equations (12) and (13) show that the wave inside the burner i is completely determined by the value of $A_{u,i}$. Using the continuity of pressure at the 'T' intersection (Eq. (10)), $A_{u,i}$ can be expressed as a function of A_{i+1} , the wave amplitude in part $i + 1$ of the annular chamber:

$$A_{u,i} = A_{i+1} / \cos(k_u l_i) \quad (14)$$

where we have assumed that $\cos(k_u l_i) \neq 0$. Eq. (14) can be reported into the two other 'T' intersection conditions (Eqs. (9) and (11)), eliminating the wave amplitude $A_{u,i}$ from the system and leading to a 2×2 linear system linking the wave amplitudes A and B in the section i of the chamber to those in section $i + 1$:

$$\begin{bmatrix} A_i \\ B_i \end{bmatrix} = T_i \begin{bmatrix} A_{i+1} \\ B_{i+1} \end{bmatrix} \quad (15)$$

T_i is called the transfer matrix and writes as:

$$T_i = R(\beta_i) + 2\Gamma_i \begin{bmatrix} -\sin(\beta_i) & 0 \\ \cos(\beta_i) & 0 \end{bmatrix} \quad (16)$$

$R(\beta_i)$ is a rotation matrix of angle $\beta_i = k d_i$ describing the waves traveling inside the part i of the chamber. The second term describes the influence of burner i on waves inside the chamber. Γ_i is a coupling factor defined by:

$$\Gamma_i = \frac{1}{2} \frac{s_i}{S} \frac{\rho^0 c^0}{\rho_u^0 c_u^0} \tan(k_u l_i) (1 + n_i e^{j\omega\tau_i}) \quad (17)$$

The coupling factor Γ_i depends both on geometrical parameters, on gas characteristics, on the flame i characteristics (described by n_i and τ_i) and also on the wave pulsation ω (through the flame transfer function and the wavenumber in unburnt gases $k_u = \omega/c_u^0$).

3.2. Dispersion relation

Equation (15) can be repeated through the N burners and periodicity imposes that:

$$\begin{bmatrix} A_1 \\ B_1 \end{bmatrix} = \left(\prod_{i=1}^N T_i \right) \cdot \begin{bmatrix} A_1 \\ B_1 \end{bmatrix} \quad (18)$$

System Eq. (18) leads to non-null solutions if and only if its determinant is null, leading to the following dispersion relation, where I_d is the identity

matrix:

$$\det \left(\prod_{i=1}^N T_i - I_d \right) = 0 \quad (19)$$

The dispersion relation Eq. (19) uses a determinant of a 2×2 matrix instead of a $4N \times 4N$. The product of the N transfer matrixes T_i is needed but this is not a problem since they are all known.

3.3. Mode structures

Once the eigenfrequencies have been obtained, mode structures can be easily found using Eq. (18). By noting $T = \prod_{i=1}^N T_i$ the product of the transfer matrixes, B_1 can be expressed as a function of A_1 as:

$$B_1 = \frac{1 - T_{11}}{T_{12}} A_1 \quad (20)$$

using for example the first line of Eq. (18).

The expression of A_i and B_i in other parts of the chambers can be obtained as a function of A_1 using the transfer matrixes and Eq. (20). As a consequence mode structures in the whole chamber are known.

Another useful decomposition of pressure and velocity fluctuation can be written using two traveling waves:

$$p'_i(x, t) = (A_i^+ e^{j k x} + A_i^- e^{-j k x}) e^{-j \omega t} \quad (21)$$

$$\rho^0 c^0 u'_i(x) = (A_i^+ e^{j k x} - A_i^- e^{-j k x}) e^{-j \omega t} \quad (22)$$

where A_i^+ and A_i^- are amplitudes of turning modes in clockwise and counter clockwise direction respectively. The wave amplitude A_i^+ and A_i^- are linked to A_i and B_i by:

$$A_i = A_i^+ + A_i^- \quad (23)$$

$$B_i = j(A_i^+ - A_i^-) \quad (24)$$

and the ratio between A_i^+ and A_i^- is given by:

$$\frac{A_i^+}{A_i^-} = \frac{1 - j B_i/A_i}{1 + j B_i/A_i} \quad (25)$$

3.4. Analytical solution in the low coupling limit

Due to significant non linearities, Eq. (19) can not generally be analytically solved. However an asymptotic solution can be determined for low coupling factors, i.e. assuming that $\forall i, |\Gamma_i| \ll 1$. In this case, the transfer matrixes (T_i in Eq. (16)) are closed to the rotation matrixes $R(\beta_i)$. As a consequence, the eigenfrequencies of the system will be close to the case of a simple annular duct and one can write:

$$kL = p\pi + \epsilon_p \quad (26)$$

with $\epsilon_p \ll p\pi$. The order of the mode is noted $p \in \mathbf{N}$. As seen in the examples (Section 6 to 8), using this low coupling assumption to calculate the dispersion relation leads to a quadratic equation for ϵ_p which can easily be solved. One should note that the low coupling assumption does not mean low thermo-acoustic coupling ($n_i \ll 1$), see Eq. (17). Except for Section 8, the low coupling assumption is valid because $s_i/S \ll 1$, $(\rho^0 c^0)/(\rho_u^0 c_u^0) = O(1)$, $\tan(k_u l_i) \ll 1$ (because $l_i \ll L$ and $k \sim p\pi/L$) and $(1 + n_i e^{j\omega\tau_i}) = O(1)$.

4. Comparison with a 3D acoustic code

Eigen frequencies and mode structures will be compared to results obtained with AVSP, a parallel 3D code devoted to the resolution of acoustic modes of industrial combustion chambers [16]. It solves the eigenvalues problem issued from a discretization on unstructured meshes of a Helmholtz equation with a source term due to the flames. The flame-acoustic interaction is taken into account via a $n - \tau$ model [35]. The local reaction term is expressed in burner i as:

$$\dot{\omega}_i = n_{u,i} e^{j\omega\tau_i} w'(\mathbf{x}_{ref,i}) \quad (27)$$

The local interaction index $n_{u,i}$ describes the local flame-acoustic interactions. In this approach flames are distributed over zones where the value of $n_{u,i}$ is non zero. To use AVSP for compact flames and check the model of Section 2, the thickness of the flame zones has been reduced as much as possible (Fig. 4). The values of $n_{u,i}$ were assumed to be constant in the flame zone i and have been chosen in order to recover the global value of interaction index n_i of the infinitely thin flame when it was properly integrated over the flame zone i [16]. The heat release fluctuations in each flame zone are driven

by the velocity fluctuations at the reference points $\mathbf{x}_{\text{ref},i}$ located in the corresponding burner. In the infinitely thin flame model these reference points are the same as the flame locations z_f . In AVSP simulations, the reference points were placed a few millimeters upstream of the flames (Fig. 4).

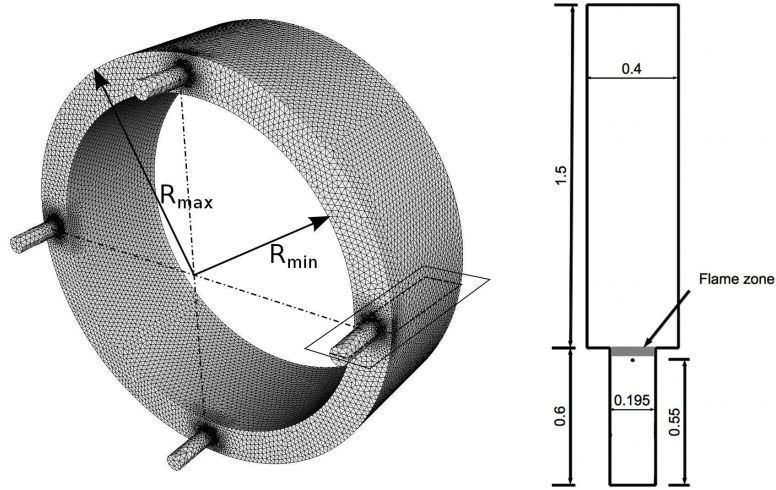


Figure 4: Academic geometry used with AVSP. The number of burners have been arbitrary set to four. Left: complete geometry. Right: plane cut in a burner. The dot located upstream of the flames denotes the position of the reference point $\mathbf{x}_{\text{ref},i}$ and the flame zone is in gray. Dimension are in meters.

The 3D geometry (Fig. 4) is constructed to match the assumption used in the 1D analytical model: the mean radius R of the cylindrical chamber is derived from the the half perimeter L of the analytical model and the $R_{\text{max}}/R_{\text{min}}$ ratio is chosen as close to one in order to reduce three dimensional effects. As the flame zone takes a minimal volume, the length of burners l_i has been slightly increased to fix the reference points positions $\mathbf{x}_{\text{ref},i}$ at the end of burners in the 1D model (see Fig. 4 and Table 1). The boundary conditions have been chosen as impermeable walls everywhere.

5. One burner

5.1. Dispersion relation and eigenfrequencies

Consider first the case $N = 1$ where only one burner is connected to the chamber (Fig. 5). Even though this is not a realistic configuration, this case is useful to understand more complex cases ($N > 1$).

The perimeter of the annular chamber $2L$, the angular position θ and position x inside the chamber are linked by:

$$x = L \frac{\theta}{\pi} \quad (28)$$

where $\theta = 0$ corresponds to the single burner position.

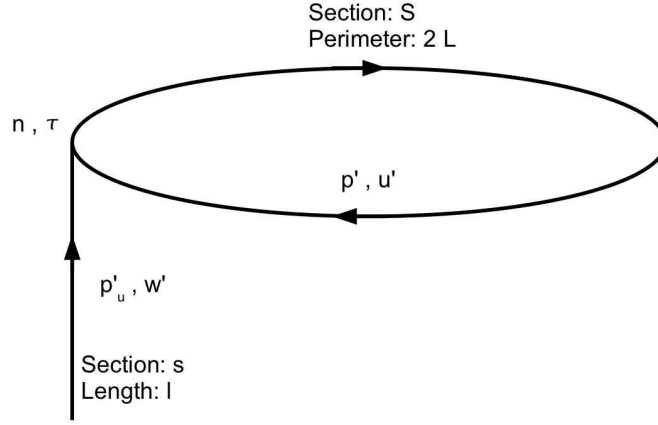


Figure 5: Configuration with a single burner connected to an annular chamber - $N = 1$.

The coupling factor between the burner and the chamber writes:

$$\Gamma = \frac{1}{2} \frac{s}{S} \frac{\rho^0 c^0}{\rho_u^0 c_u^0} \tan(k_u l) (1 + n e^{j\omega\tau}) \quad (29)$$

and the transfer matrix is:

$$T = \begin{bmatrix} \cos(2kL) & -\sin(2kL) \\ \sin(2kL) & \cos(2kL) \end{bmatrix} + 2\Gamma \begin{bmatrix} -\sin(2kL) & 0 \\ \cos(2kL) & 0 \end{bmatrix} \quad (30)$$

Using Eq. (19), the dispersion relation becomes:

$$\sin^2(kL) = -\Gamma \cos(kL) \sin(kL) \quad (31)$$

Equation. (31) is transcendental and Γ depends on the pulsation ω . Assuming a low coupling factor (Eq. (26) with $\epsilon_p \ll p\pi$), the dispersion relation Eq. (31) becomes:

$$\epsilon_p^2 + \Gamma_p^0 \epsilon_p = 0 \quad (32)$$

where Γ_p^0 is the value of Γ when $kL = p\pi$ (i.e. $\omega = \omega_p^0 = p\pi c^0/L$):

$$\Gamma_p^0 = \frac{1}{2} \frac{s}{S} \frac{\rho^0 c^0}{\rho_u^0 c_u^0} \tan\left(p\pi \frac{c^0 l}{c_u^0 L}\right) (1 + n e^{j\omega_p^0 \tau}) \quad (33)$$

Equation (32) has two solutions:

$$\epsilon_p = \begin{cases} 0 \\ -\Gamma_p^0 \end{cases} \quad (34)$$

The first mode ($\epsilon_p = 0$) is a standing mode while the second one ($\epsilon_p = -\Gamma_p^0$) will be called mixed because it is a superposition of standing and rotating modes. These solutions are summarized in Table 2 and discussed in Section 5.2 and 5.3.


Case	Frequencies	Stability condition	A^+/A^- ratio	Type
	$\epsilon_p = 0$	neutral	-1	standing
	$\epsilon_p = -\Gamma_p^0$	$\sin(\omega_p^0 \tau) > 0$	$1 + j 2 \Gamma_p^0$	mixed

Table 2: Modes for 1 burner.

5.2. Standing mode

A first solution is $\epsilon_p = 0$, corresponding to $k = p\pi/L$ and p' and u' given by:

$$p'(\theta, t) = B \sin(p\theta) e^{-j\omega_p^0 t} \quad (35)$$

$$\rho^0 c^0 u'(\theta, t) = -j B \cos(p\theta) e^{-j\omega_p^0 t} \quad (36)$$

$A = 0$ and B is a degree of freedom. Mode structure of pressure fluctuation is plotted in Fig. 6. The burner is located at a pressure node and a velocity

antinode. According to Eq. (14) there is no wave inside the burner since $A = 0$; thus the chamber is not influenced by the burner except by the fact that the burner connected to the chamber must be located at a pressure node. The frequency is $f_p = p c^0 / (2L)$ and has no imaginary part: the mode is neutral. Pressure mode structure obtained with AVSP is compared with Eq. (35) in Fig. 6. A very good agreement is found.

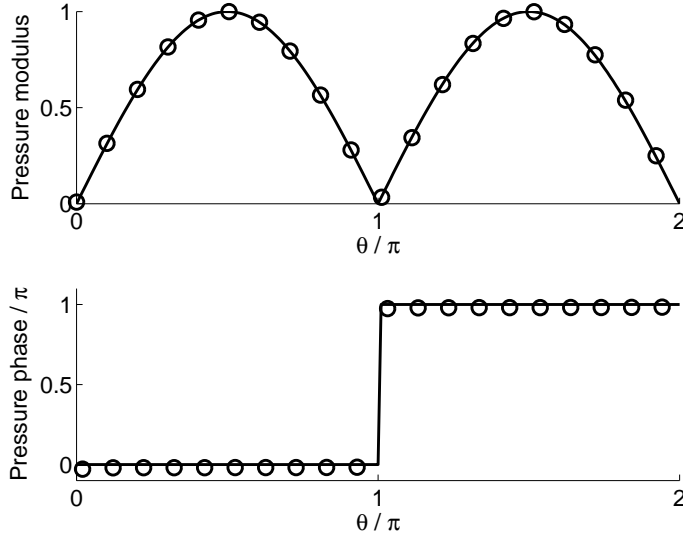


Figure 6: $N = 1$ - First ($p = 1$) mode structure of pressure in the annular chamber for the neutral standing mode ($\epsilon_1 = 0$) for a delay $\tau = 8 \text{ ms}$. The single burner is located at $\theta = 0$. — : model prediction Eq. (35), O: AVSP results.

Using $A = 0$ into Eq. (23) leads to a ratio $A^+ / A^- = 1$ for the traveling wave decomposition (Eqs. (21) and (22)) showing that the mode is a standing mode due to the superposition of rotating modes with equal amplitudes.

5.3. Mixed mode

The other solution for a single burner ($N = 1$) (Table 2) is given by $\epsilon_p = -\Gamma_p^0$. The corresponding frequency is:

$$f_p = \frac{c^0}{2L} \left(p - \frac{\Gamma_p^0}{\pi} \right) \quad (37)$$

Solution of Eq. (37) for the first two modes ($p = 1$ and 2) as a function of τ are compared to results obtained with AVSP in Figs. 7 to 10. The flame

interaction index n is fixed to its theoretical value in the low frequency limit ($n = T^0/T_u^0 - 1 \simeq 1.57$) and all other numerical values are given in Table 1, leading to small values for Γ_p^0 ($|\Gamma_1^0| < 0.02$ and $|\Gamma_2^0| < 0.04$). The revolution time $\tau_r = c^0/(2L)$ is used as a scaling factor for τ in Figs. 7 to 10.

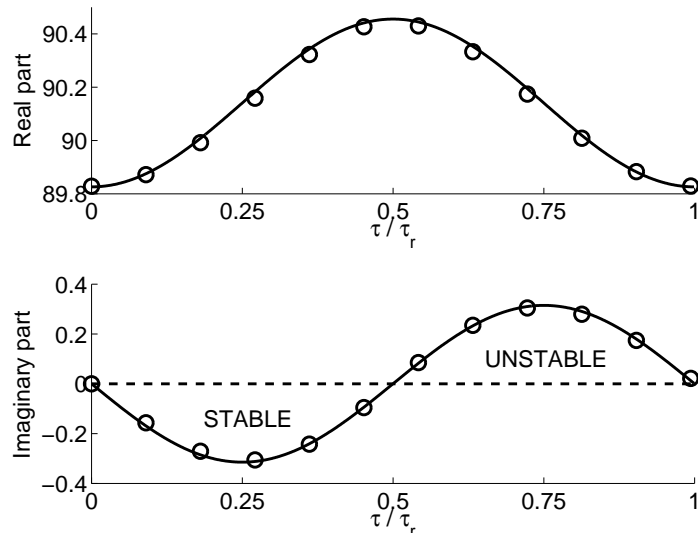


Figure 7: $N = 1$ - Eigenfrequency of the mixed mode of first order ($p = 1$) for one burner as a function of τ/τ_r . — : model prediction Eq. (37), \circ : AVSP results.

A very good agreement between theoretical prediction and numerical simulation is found for the first mode ($p = 1$), both for the real part and imaginary part of the eigenfrequencies (Fig. 7). Figure 8 shows that the eigenfrequency describes a circle in the complex plane when the value of τ is changing, as predicted by Eq. (37) because of the term $e^{j\omega_p^0\tau}$ in the definition of Γ_p^0 , Eq. (33).

A good agreement is also found for the second mode ($p = 2$). The real part of the frequency is predicted with an accuracy superior than 1% but the circle seems to be right shifted and to have a too small radius. The authors attribute this discrepancy to the 3D effects and to the flame description - in particular in the fact that z_f differs of l by 10%. Comparison between Fig. 7 and Fig. 9 shows that maximum values of the imaginary part of f_2 are larger than for f_1 showing that mode 2 is more unstable than mode 1. Since $c^0 l \ll c_u^0 L$, it follows from Eqs. (33) and (37) that the frequency of order p

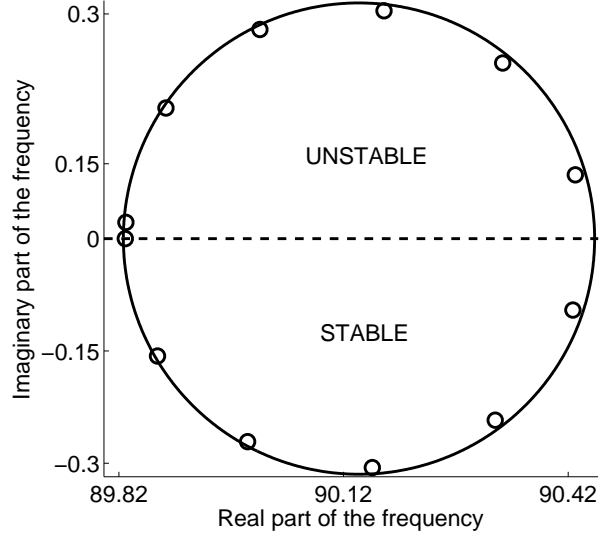


Figure 8: $N = 1$ - Variation of the eigenfrequency of the mixed mode of first order ($p = 1$) in the complex plane when τ is changing. — : model prediction Eq. (37), \circ : AVSP results.

can be approximated by:

$$f_p \simeq p \frac{c^0}{2L} \left(1 - \frac{1}{2} \frac{s}{S} \frac{l}{L} \frac{\rho^0}{\rho_u^0} \left(\frac{c^0}{c_u^0} \right)^2 (1 + n e^{j\omega_p^0 \tau}) \right) \quad (38)$$

Equation (38) shows that the imaginary part of the azimuthal mode of order p is proportional to p . As a consequence time amplification of higher order modes are greater than of low order modes in this model where dissipative effects have been neglected.

Figures 7 and 9 show that Eq. (37) predicts the sign of the imaginary part of the eigenfrequencies for the first two modes precisely and can be used to predict the stability of this simple system. The corresponding stability criterion is quite simple:

$$\sin(\omega_p^0 \tau) > 0 \quad (39)$$

or using the revolution time $\tau_r = c^0/(2L)$:

$$\sin(p 2\pi \frac{\tau}{\tau_r}) > 0 \quad (40)$$

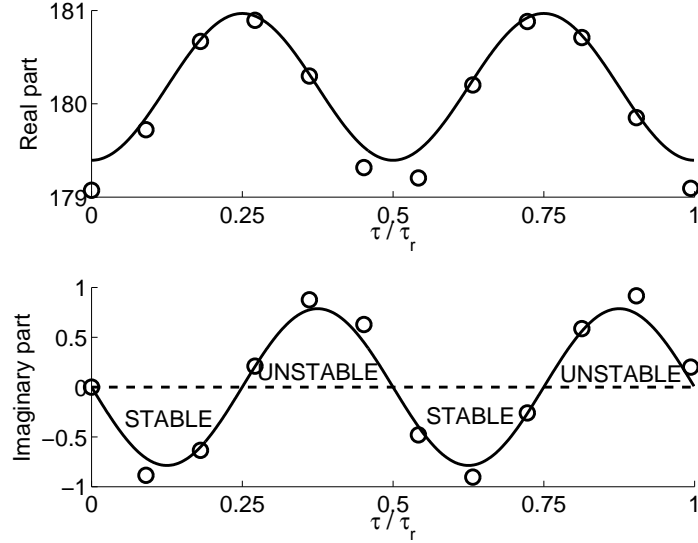


Figure 9: $N = 1$ - Eigenfrequency of the mixed mode of second order ($p = 2$) for one burner as a function of τ/τ_r . —: model prediction Eq. (37), \circ : AVSP results.

Equation (40) shows that the first mode is stable when $\tau < \tau_r/2$; thus the first azimuthal mode is amplified when the flame delay is larger than $\tau_r/2$ where τ_r is the first azimuthal mode period. It is interesting to note that this instability criteria ($\tau > \tau_r/2$) is also the one found in simple models for longitudinal combustion instabilities in straight ducts [12].

The pressure and velocity mode structures for the first mode ($p = 1$) corresponds to:

$$p'(\theta) = A \left(\cos(\theta(p - \Gamma_p^0/\pi)) - \Gamma_p^0 \sin(\theta(p - \Gamma_p^0/\pi)) \right) \quad (41)$$

$$\rho^0 c^0 u'(\theta) = jA \left(\sin(\theta(p - \Gamma_p^0/\pi)) + \Gamma_p^0 \cos(\theta(p - \Gamma_p^0/\pi)) \right) \quad (42)$$

Results for pressure are compared to AVSP in Fig. 11. A very good agreement is found between the analytical solution and AVSP results. The burner position ($\theta = 0$) corresponds to an antinode of pressure but is not a node of velocity ($u'(0) = j A \Gamma_p^0 \neq 0$).

The ratio between B and A is fixed to $B = -A \Gamma_p^0$, corresponding for A^+/A^- in the traveling wave decomposition (Eqs. 21 and 22) to:

$$\frac{A^+}{A^-} = 1 + j 2 \Gamma_p^0 \quad (43)$$

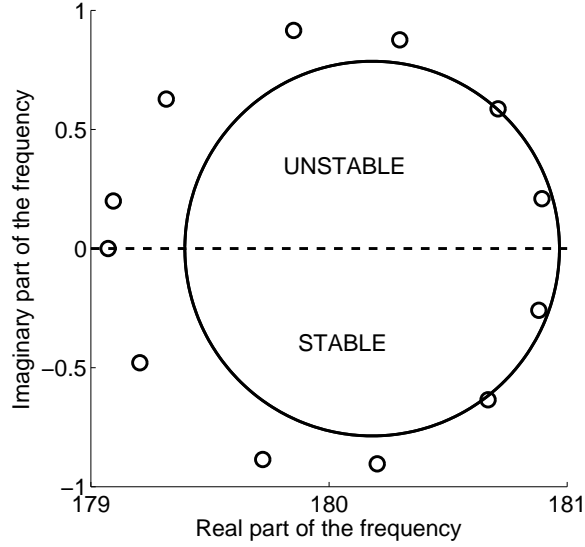


Figure 10: $N = 1$ - Variation of the eigenfrequency of the mixed mode of second order ($p = 2$) in the complex plane when τ is changing. — : model prediction Eq. (37), \circ : AVSP results.

Application of Eq. (43) to numerical values of Table 1 with $\tau = 8 \text{ ms}$ gives $A^+/A^- \simeq 1.02 - 0.010j$; this frequency does not correspond to a purely standing wave. As shown in Appendix A, the pressure and the velocity are symmetric despite the fact that the ratio A^+/A^- has not a modulus equal to one. Because the wavenumber is not real valued ($k_i \neq 0$), this ratio depends on the (arbitrary chosen) origin of the x coordinate; a suitable choice which leads to $A^+ = A^-$ is identified in Appendix A which also establishes that the mode corresponding to Eq. (43) shares the same symmetry than the configuration itself. It is also shown that this solution is neither a purely standing nor purely propagation mode. Thus the fact that Eq. (43) corresponds to a single mode (the corresponding frequency is not degenerate and is a single root of the dispersion relation) is not in contradiction with geometrical considerations and study of Evesque et al. [36] (which deals only with modes where the imaginary part of the frequency is null).

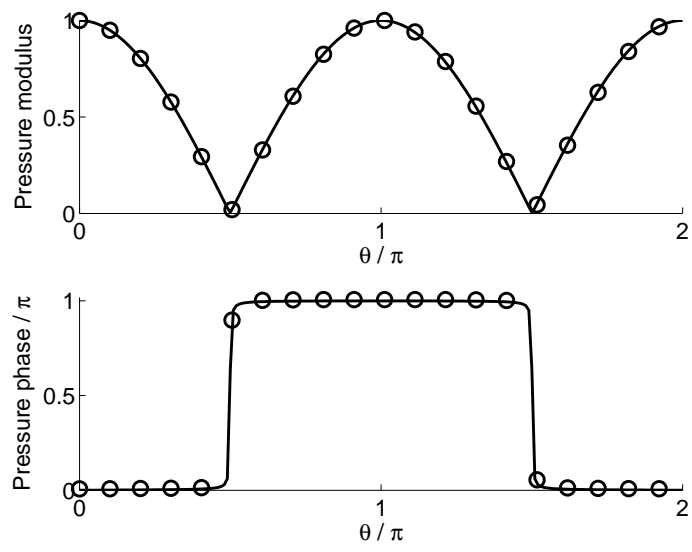


Figure 11: $N = 1$ - First ($p = 1$) mode structure of pressure in the annular chamber of the unstable mode for a delay $\tau = 8 \text{ ms}$. Burner is located at $\theta = 0$. — : model prediction Eq. (41), \circ : AVSP results.

6. Two burners

We consider now the case of two burners ($N = 2$) of same section s and same length l , symmetrically disposed ($d_1 = d_2 = L$) on an annular chamber but with different flame transfer functions ($(n_1, \tau_1) \neq (n_2, \tau_2)$). The dispersion relation is obtained using Eq. (19):

$$(1 - \Gamma_1 \Gamma_2) \sin^2(kL) = -(\Gamma_1 + \Gamma_2) \cos(kL) \sin(kL) \quad (44)$$

Using low coupling hypothesis, Eq. (44) becomes:

$$\epsilon_p^2 + (\Gamma_{p,1}^0 + \Gamma_{p,2}^0) \epsilon_p = 0 \quad (45)$$

where $\Gamma_{p,i}^0$ is the value of Γ_i for $\omega = \omega_p^0 = p\pi c/L$. Equation (45) has two solutions (Table 3):

$$\epsilon_p = \begin{cases} 0 \\ -(\Gamma_{p,1}^0 + \Gamma_{p,2}^0) \end{cases} \quad (46)$$

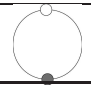
Case	Frequencies	Stability condition	A_1^+/A_1^-	A_2^+/A_2^-
	$\epsilon_p = 0$	neutral	-1	-1
	$\epsilon_p = -(\Gamma_{p,1}^0 + \Gamma_{p,2}^0)$	$n_1 \sin(\omega_p^0 \tau_1) + n_2 \sin(\omega_p^0 \tau_2) > 0$	$1 + j 2 \Gamma_{p,2}^0$	$1 + j 2 \Gamma_{p,1}^0$

Table 3: Modes for 2 burners.

The first solution ($\epsilon_p = 0$) corresponds to a standing neutral mode where burners are located at pressure nodes and no activity exists within the burners ($A_{u,i} = 0$). Expressions of pressure and velocity fluctuations are identical to Eqs. (35) and (36). The second solution corresponds to a complex mode where the stability condition is:

$$n_1 \sin(\omega_p^0 \tau_1) + n_2 \sin(\omega_p^0 \tau_2) > 0 \quad (47)$$

Fig. 12 shows the stability zones for the first two modes ($p = 1$ and $p = 2$) given by Eq. (47) when $n_1 = n_2$: for any value of τ_1 , one or more values of τ_2 can be chosen in order to ensure the stability of the first mode. The same could be said for the second mode. But in order to ensure the stability of both first and second modes, τ_1 should satisfy $w_1^0 \tau_1 < 3\pi/2$ or $w_1^0 \tau_1 > 7\pi/4$ (if $w_1^0 \tau_1 > 2\pi$ these conditions should be translated to 2π). This conclusion has a serious impact on stability control: it is not always possible to control the stability of the whole system only by changing the value of the delay of one of the two flames.

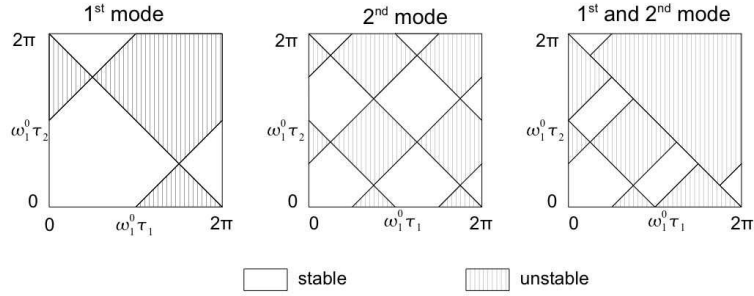


Figure 12: $N = 2$ - Stability diagrams for the first and second mode of an annular chamber with two burners having equal interaction indices $n_1 = n_2$.

7. Four burners

The method described above can be applied to any number of burners. It is interesting to consider the case $N = 4$ because it allows us to investigate passive control techniques. We consider here the case of four burners and investigate a usual method applied in certain gas turbines: break the symmetry of the system by using two different types of burners and placing them to damp azimuthal modes. Starting from a configuration with four identical burners that lead to an unstable first mode, the objective is to modify the FTF of two of the four burners to damp azimuthal modes. Each type of burner has a specific FTF. Modified burners can be disposed either symmetrically or side by side (Fig. 13).

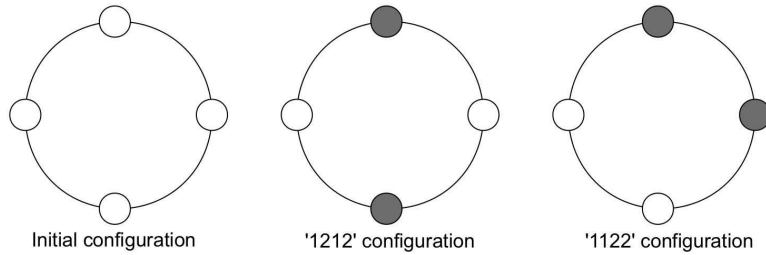


Figure 13: Geometrical arrangement of the four burners with two different flame transfer functions: (n_1, τ_1) in white and (n_2, τ_2) in gray.

The characteristics of the flame transfer functions are noted (n_1, τ_1) for the initial burners and (n_2, τ_2) for the modified burners. The two geometrical

dispositions ('1212' and '1122') of Fig. 13 will be studied to compare their impact on the stability of the system when the time delay τ_2 is changing.

7.1. Initial configuration: four identical burners of type 1

The initial configuration consists in four burners placed along the chamber (Fig. 13), with a flame transfer function given by (n_1, τ_1) . Using Eq. (19) with the low coupling limit assumption leads to:

$$\epsilon_1^2 + 4\Gamma_{1,1}^0 \epsilon_p + 4(\Gamma_{1,1}^0)^2 = 0 \quad (48)$$

The dispersion relation Eq. (48) leads here to a double root for the eigenfrequencies of the first mode:

$$\epsilon_1 = \begin{cases} -2\Gamma_{1,1}^0 \\ -2\Gamma_{1,1}^0 \end{cases} \quad (49)$$

In this case the ratios B_i/A_i (or equivalently A_i^+/A_i^-) are fixed by non-linear effects which are not taken into account in our analysis. The mode observed for this case can be standing ($|A_i^+| = |A_i^-|$), turning ($A_i^+ = 0$ or $A_i^- = 0$) or a combination of these modes as observed for example in the 360° LES of Wolf et al. [27].

Looking at the imaginary part of the frequency, Eq. (49) leads to the stability condition for the first mode:

$$\sin(\omega_1^0 \tau_1) > 0 \quad (50)$$

As we assume that this mode is unstable, we choose the particular value of $\tau_1 = 7 \text{ ms}$ for numerical applications, corresponding to $\tau_1/\tau_r \simeq 0.58$ and $\sin(\omega_1^0 \tau_1) \simeq -0.5$.

7.2. '1212' configuration

This configuration corresponds to the case where two burners of type '1' symmetrically disposed have been replaced by two burners of type '2' with flame transfer functions given by (n_2, τ_2) (Fig. 13). In the low coupling limit, two distinct eigenfrequencies are found from the resolution of Eq. (19):

$$\epsilon_1 = \begin{cases} -2\Gamma_{1,1}^0 \\ -2\Gamma_{1,2}^0 \end{cases} \quad (51)$$

The first solution ($\epsilon_1 = -2\Gamma_{1,1}^0$) is only depending on the flame transfer function of the initial burners: this mode can not be controlled using the burners of kind '2'. Its stability condition is:

$$\sin(\omega_1^0 \tau_1) > 0 \quad (52)$$

As the initial configuration was assumed to be unstable, this frequency will remain unstable even if two burners are replaced.

The second solution ($\epsilon_2 = -2\Gamma_{1,2}^0$) depends only on the flame transfer function of the modified burners. Its stability is given by the value of τ_2 :

$$\sin(\omega_1^0 \tau_2) > 0 \quad (53)$$

The variation of the two eigenfrequencies with τ_2 are plotted in Figs. 14 and 15 where the comparison with AVSP results are made. As predicted by the theory, one of the eigenfrequency is independent of τ_2 while the other describes a circle in the complex plane.

Pressure modes structures obtained with AVSP for $\tau_2 = 0.67 \tau_r$ ($\tau_2 = 8 \text{ ms}$) are given in Fig. 16.

7.3. '1122' configuration

This configuration corresponds to the case where the burners of type '2' are disposed side by side (Fig. 13). In the low coupling limit, a double eigenfrequency is found:

$$\epsilon_1 = \begin{cases} -(\Gamma_{1,1}^0 + \Gamma_{1,2}^0) \\ -(\Gamma_{1,1}^0 + \Gamma_{1,2}^0) \end{cases} \quad (54)$$

The solution depends on the FTF of the two burner types '1' and '2' so that (contrary to the '1212' case) it is possible to control the mode using type '2' burners. Assuming for example that type '2' burners will differ from type '1' burners only through their delay ($\tau_2 \neq \tau_1$ but $n_2 = n_1$), the stability condition writes:

$$\sin(\omega_1^0 \tau_1) + \sin(\omega_1^0 \tau_2) > 0 \quad (55)$$

The stability of the system can be obtained by changing the value of τ_2 : the variation of the two eigenfrequencies with τ_2 are plotted in Figs. 17 and 18 when $\tau_1/\tau_r = 0.58$ and compared to AVSP predictions. For each value of τ_2 AVSP gives two distinct eigenfrequencies while the theory predicts only one value. However these values are both very close to the theoretical prediction

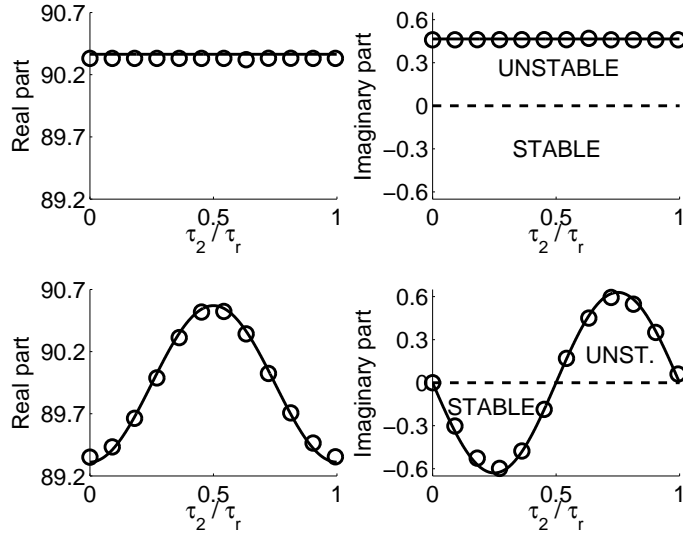


Figure 14: $N = 4$ - Variation of the first (top) and second (bottom) eigenfrequency of the first mode for the '1212' configuration as a function of τ_2 ($\tau_1 = 7 \text{ ms}$). — : model predictions Eq. (51), \circ : AVSP results.

(Figs. 17 and 18). Using Fig. 17, when the delay of the type '2' burners changes between $0.13 \tau_r$ and $0.37 \tau_r$ all modes become stable. These results suggest that passive control of azimuthal mode by mixing different burners can work if the modified burners are located one near the other ('1122' case) and not apposite to each other ('1212' case).

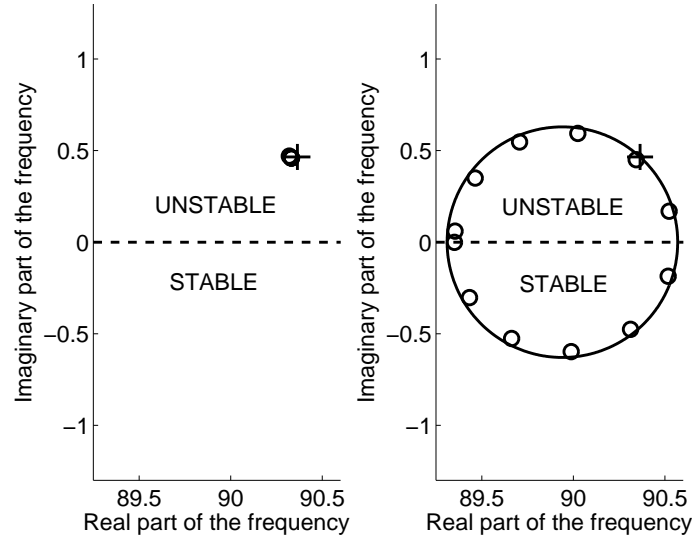


Figure 15: $N = 4$ - Variation of the first (left) and second (right) eigenfrequency of the first mode in the complex plane for the '1212' configuration when τ_2 is changing and $\tau_1 = 7 \text{ ms}$. — : model prediction Eq. (51), \circ : AVSP results, $+$: mode with 4 identical burners Eq. (49).

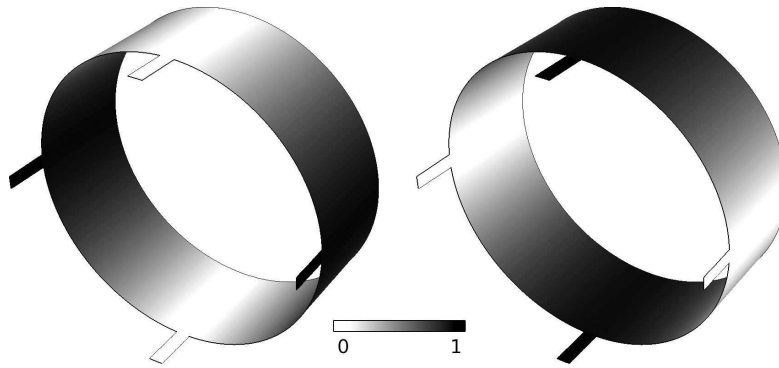


Figure 16: $N = 4$ - Pressure modulus of the first mode ($p = 1$) obtained with AVSP in the '1212' configuration with $\tau_1 = 7 \text{ ms}$ and $\tau_2 = 8 \text{ ms}$. Left and right correspond to the two eigenfrequencies.

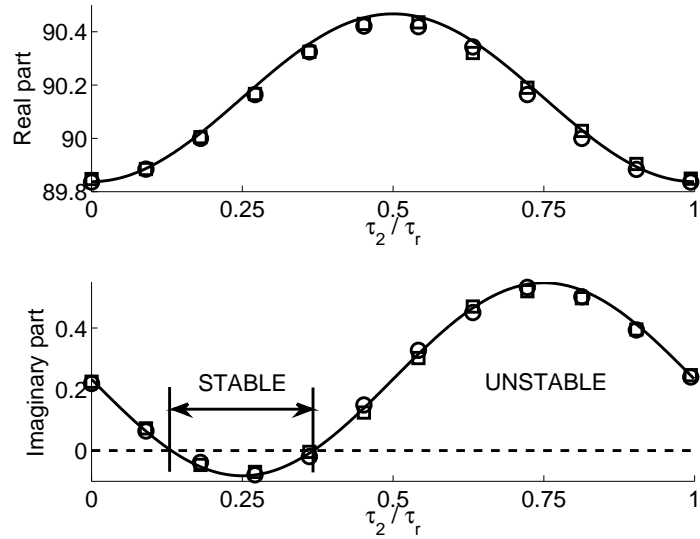


Figure 17: $N = 4$ - Variation of the eigenfrequency of the first mode for the '1122' configuration as a function of τ_2 ($\tau_1 = 7$ ms). — : model prediction Eq. (54), \circ and \square : AVSP results.

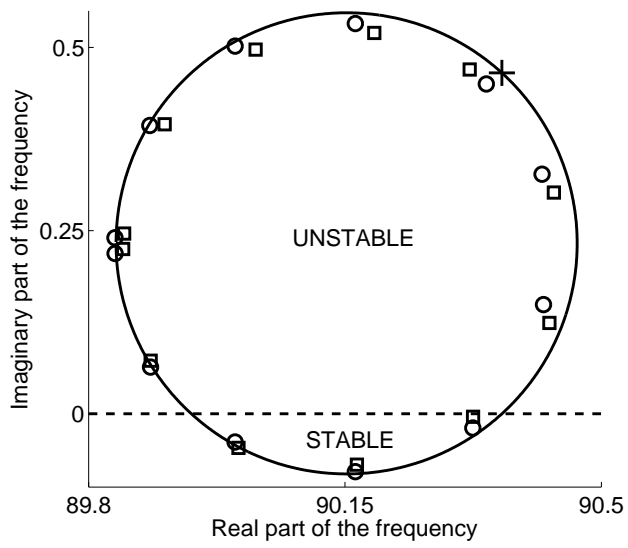


Figure 18: $N = 4$ - Variation of the eigenfrequency of the first mode in the complex plane for the '1122' configuration when τ_2 is changing and $\tau_1 = 7$ ms. — : model prediction Eq. (54), \circ and \square : AVSP results, + : mode with 4 identical burners Eq. (49).

8. Application to a real configuration

Previous sections have compared results obtained with the 3D Helmholtz solver and the 1D description in the low coupling limit on academic configurations (Fig. 4). In this section a 3D complex geometry is studied, corresponding to a full annular reverse flow helicopter combustion chamber. The configuration is described in Section. 8.1. The eigenfrequencies computed as a function of the flames delay using three methods: AVSP results on the complex geometry (Section 8.2), 1D analytical model using the low coupling assumption (Section 8.3.1) and numerical resolution of the dispersion relation of the 1D model without assuming a low coupling between burners and the chamber (Section 8.3.2). A particular attention is paid to the stability condition on the flames' delay.

8.1. Description of the target configuration

The geometry is a gas turbine demonstrator designed by Turbomeca (Safran group) and composed of 15 sectors. The whole chamber is considered, including its casing and the fifteen burners. The domain starts just downstream of the compressor, where the cold flow enters the casing. The latter then feeds the combustion chamber through swirlers that consists of two co-annular counter-rotating swirl stages, dilution holes that limits the extent of the primary zone where combustion occurs and multiperforated plates and cooling films are used to cool the liner. Burnt gases exhaust from the combustion chamber and enter the stator of the High Pressure Turbine. At that point the flow is choked. However, since the Helmholtz solver assumes zero Mach number, the computational domain is truncated slightly upstream of the outlet to fulfill this assumption. Fig. 19 displays the full annular geometry along with a transversal cut of a sector showing the main features aforementioned.

8.2. AVSP simulations

The main inputs for the Helmholtz calculations, namely sound speed and flame transfer function, are extracted from a 3D reactive Large Eddy Simulation (LES) of a single pulsed sector, following the procedure described in Kaufmann et al. [37]. A description of the LES solver used and its application on similar cases can be found in [38, 6, 27]. The frequency of the pulsation on the inlet is chosen to be 750 Hz, which is the frequency of the dominant azimuthal mode in this configuration. This single-sector calculation provides

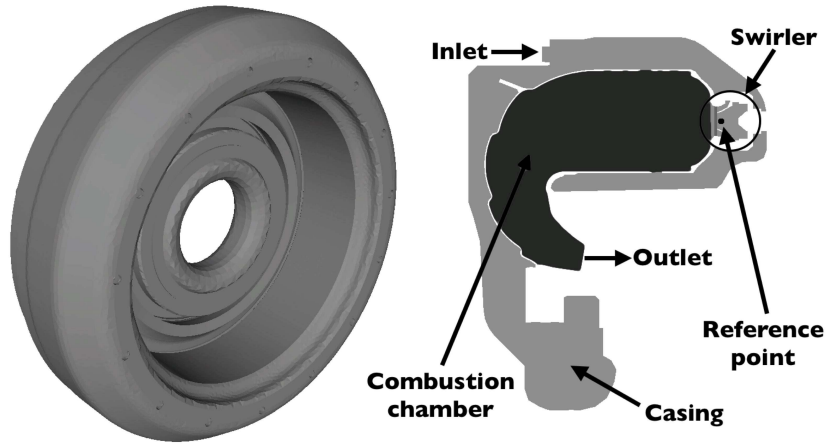


Figure 19: Computational domain: full geometry (left), transversal cut of a sector (right).

sound speed and local interaction index fields (Fig. 20) which are supposed to be independent of frequency (an assumption which should be relaxed to match experimental data outside the $700-800Hz$ range). Using the reference point shown in Fig. 19, the flame transfer function is constructed through the local interaction index and a global prescribed delay. Inlet and outlet boundary conditions are set to zero acoustic velocity. Acoustic damping by the multiperforated plates is included in the Helmholtz calculations through an homogeneous model [39, 40].

For each value of the delay τ , AVSP identifies two very close frequencies for the first mode. The real and imaginary part of one of them as a function of the delay τ are compared to analytical results in Figs. 22 to 24.

8.3. 1D description

To use the dispersion relation Eq. (19) for the geometry of Fig. 19, inputs of the analytical model are chosen accordingly to the 3D complex geometry and the operating conditions, and are shown in Fig. 21 and summarized in Table 4. In particular the equivalent interaction index n was calculated by integrating the local interaction index $n_{u,i}$ over the combustion chamber (see Section 4 and [16] for more details).

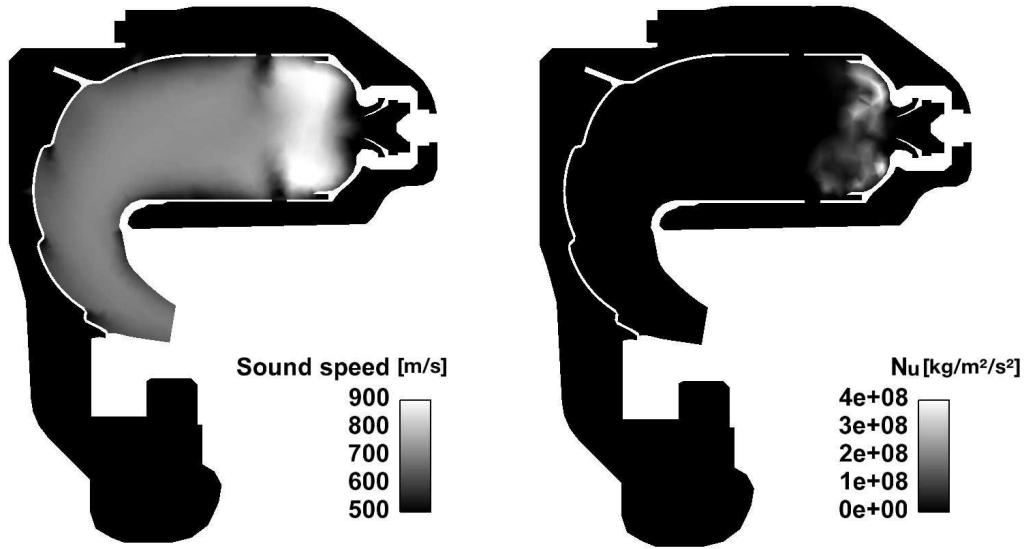


Figure 20: Sound speed (left) and local interaction index $n_{u,i}$ (right) fields on a transverse cut of a single sector.

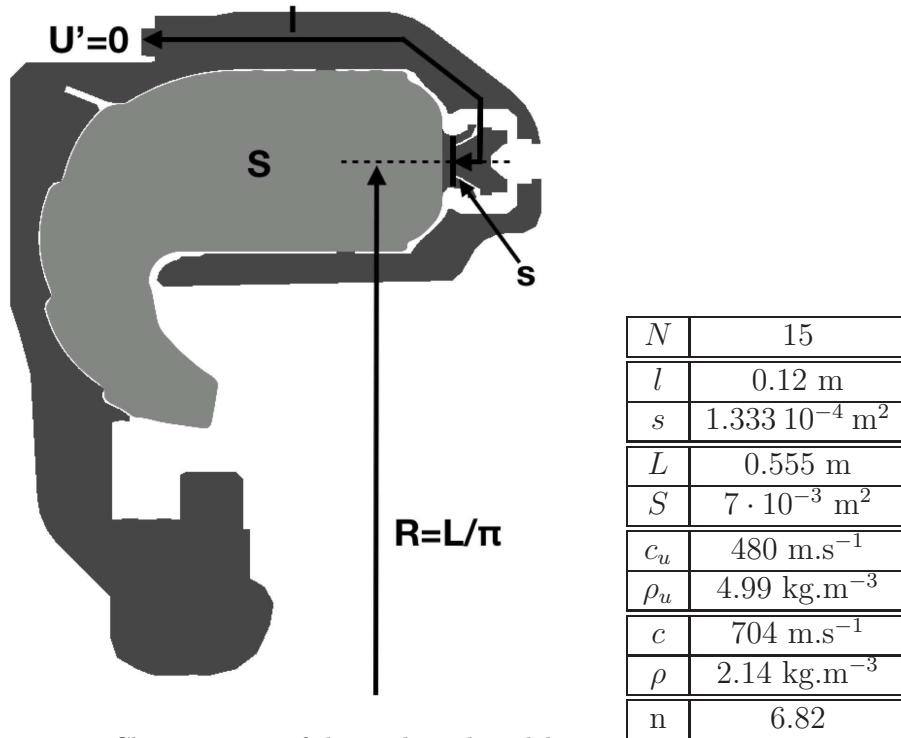


Figure 21: Chosen inputs of the analytical model calculated from the 3D complex geometry, here Table 4: Chosen values for the inputs of the analytical model.

8.3.1. Low coupling limit

In the low coupling limit, a double eigenfrequency is found for the first mode ($p = 1$):

$$\epsilon_1 = \begin{cases} -15 \Gamma_1^0 / 2 \\ -15 \Gamma_1^0 / 2 \end{cases} \quad (56)$$

Comparison of Eq. (56) with AVSP results is made in Figs. 22 and 23. The global tendency is well predicted. However, AVSP results present a dissymmetry that is not predicted by the low coupling theory. The periodicity of the eigenfrequencies for $\tau = \tau_r$ is not found in AVSP results. Moreover, the critical delay of transition from stable to unstable modes is observed for $\tau \simeq 0.38 \tau_r$ while the model predict a transition at $\tau = 0.5 \tau_r$.

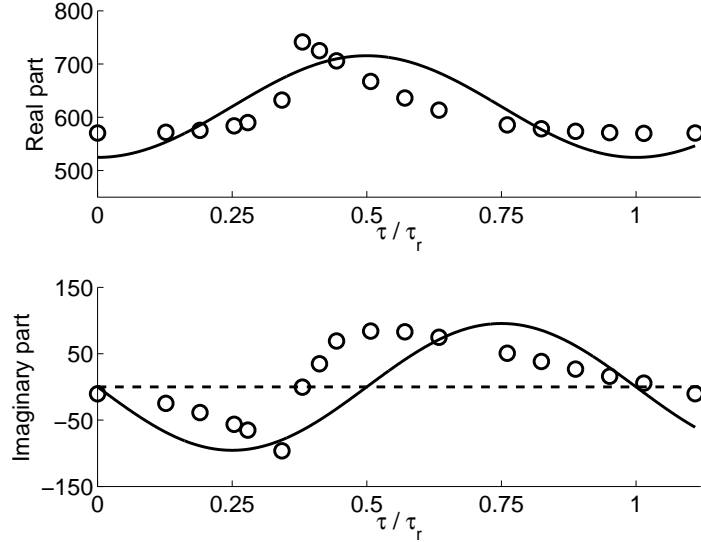


Figure 22: $N = 15$ - Eigenfrequency of the first mode ($p = 1$) for the real configuration as a function of τ/τ_r . — : model prediction Eq. (56), \circ : AVSP results.

The imaginary part of the frequency for $\tau = 0$ is predicted to be 0 while it is found to have a small negative value in AVSP. This difference is due to the damping effect of the multiperforated plates in the 3D configuration that is not taken into account in the 1D model.

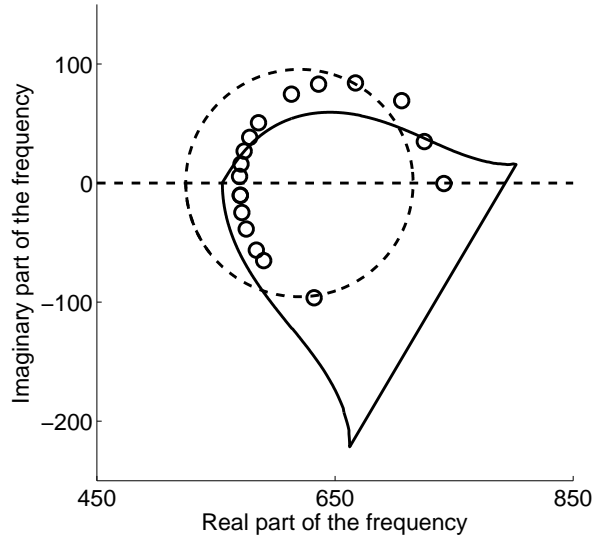


Figure 23: $N = 15$ - Variation of the eigenfrequency of the complex mode of first mode ($p = 1$) in the complex plane for the real configuration when τ is changing. --- : low coupling hypothesis Eq. (56), — : exact 1D resolution Eq. (19), \circ : AVSP results.

8.3.2. Exact 1D solution

In the previous section, the low coupling assumption was used. This hypothesis assumes that flames perturbations lead only to a small deviation of the eigenfrequencies. However, as seen in Fig. 22, the real part of the frequencies can change from 500 Hz to 800 Hz , breaking the low coupling hypothesis. This is due to the combination of a high value of interaction index ($n = 6.82$), a high number of burners ($N = 15$) and a non negligible ratio l/L , leading to values of ϵ_1 that are not small ($|\epsilon_1| \neq 0.5$). As a consequence, assuming $\epsilon_1 \ll \pi$ in the dispersion relation Eq. (19) is not justified and leads to poor results. However, using an appropriate algorithm (e.g. Newton-Raphson), the dispersion relation Eq. (19) can be numerically solved. Results obtained with this method are compared to AVSP results in Fig. 23 and 24. It is clear that predictions are improved. In particular, the shape of frequency curves is better predicted and the delay of stability transition is now found to be $\tau \simeq 0.39 \tau_r$, close to the value of $0.38 \tau_r$ given by the 3D Helmholtz solver.

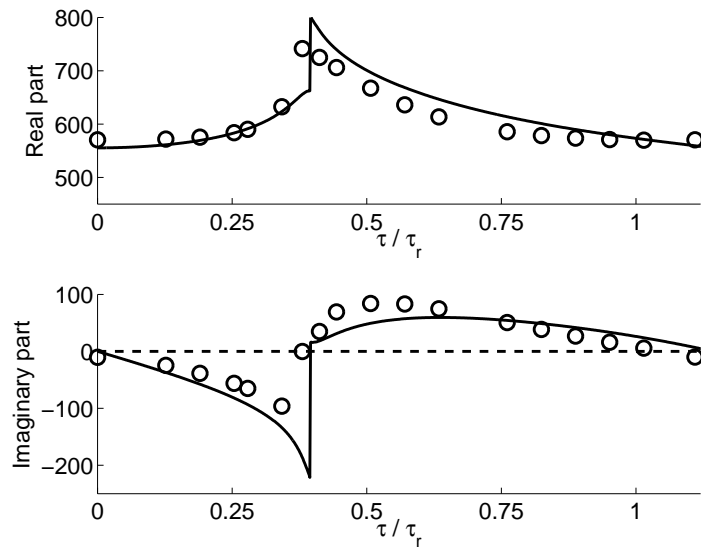


Figure 24: $N = 15$ - Eigenfrequency of the first order ($p = 1$) for the real configuration as a function of τ/τ_r . — : exact 1D resolution Eq. (19), \circ : AVSP results.

9. Conclusion

To complement expensive Large Eddy Simulation [17] and Helmholtz [16] tools used to study azimuthal modes in annular chambers, simpler tools are required to understand the physics of these modes and test control strategies [22]. This paper describes a simple analytical theory to compute the azimuthal modes appearing in these chambers. It is based on a network, zero Mach number formulation where N burners are connected to a single annular chamber. A manipulation of the corresponding acoustic equations in this configuration leads to a simple dispersion relation which can be solved by hand when the interaction indices of the flame transfer function are small and numerically when they are not. This analytical tool has been compared systematically to a full three-dimensional Helmholtz solver and very good agreement was found. The academic test cases included a model annular chamber fed by a single burner ($N = 1$), two burners ($N = 2$) and four burners ($N = 4$). In this last case, it was shown that passive control where two types of burners are mixed on the same combustor, is more efficient when the modified burners are located side by side and not on opposite positions, an observation which matches industrial recommendations when N is larger. The last test case corresponded to a complete real helicopter chamber ($N = 15$) and confirmed that, even in this complex geometry, a simple network model can predict stability maps for the azimuthal modes. These results show that building very simple analytical tools to study azimuthal modes in annular chambers is an interesting path to understand and control them.

Appendix A. Symmetry of the case $N = 1$

Dispersion relation and mode structures for the case $N = 1$ where only one burner is connected to the chamber (Fig. 5) were studied in Section 5. In particular, the solution $\epsilon_p = -\Gamma_p^0$ leads to a ratio A^+/A^- with a modulus that is not equal to one, a fact that seems to be in contradiction with basic geometrical symmetry consideration. However, Eq. (43) is an approximation valid in the low coupling limit. The exact value of the ratio is given by:

$$\frac{A^+}{A^-} = e^{-j2kL} \quad (\text{A.1})$$

Modulus of A^+/A^- is equal to one only if k is real, i.e. in the case where there is no flame ($n = 0$). Injecting Eq. (26) and $\epsilon_p = -\Gamma_p^0$ into Eq. A.1

leads to its approximate value given by Eq. (43). Injecting Eq. (A.1) into Eqs. (21) and (22) leads to the following expressions for the pressure and velocity fluctuations :

$$p'(x, t) = A^+ e^{jkL} (e^{jkx^*} + e^{-jkx^*}) e^{-j\omega t} \quad (\text{A.2})$$

$$\rho^0 c^0 u'(x, t) = A^+ e^{jkL} (e^{jkx^*} - e^{-jkx^*}) e^{-j\omega t} \quad (\text{A.3})$$

where $x^* = x - L$. Equations (A.2) and (A.3) show that the pressure is symmetric and the velocity anti-symmetric, in agreement with geometrical considerations. Thus, when the origin of the x axis is taken at the opposite side of the burner, the pressure writes as the sum of two waves of the same amplitude travelling in opposite directions. Snapshots of the real part of the pressure and velocity fluctuations are plotted on Figures A.25 and A.26 at different instants, illustrating the symmetry of the pressure. The maximum of the pressure increases because the mode is unstable ($\omega_i > 0$). The mode is not a standing mode but is not a spinning mode neither.

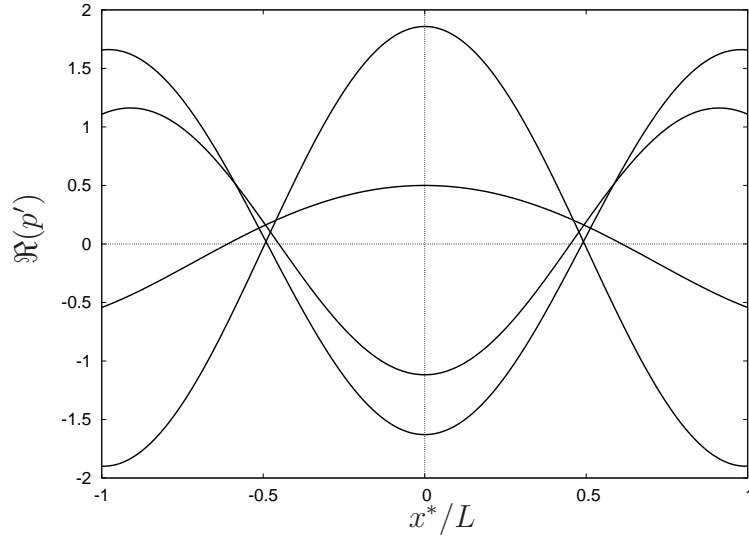


Figure A.25: $N = 1$ - Snapshots of the pressure fluctuation at different instants for the first mode ($p = 1$) and $\epsilon_1 = 0.1 + 0.2j$. A^+ was set to 1. The injector is positioned at $x^*/L \pm 1$.

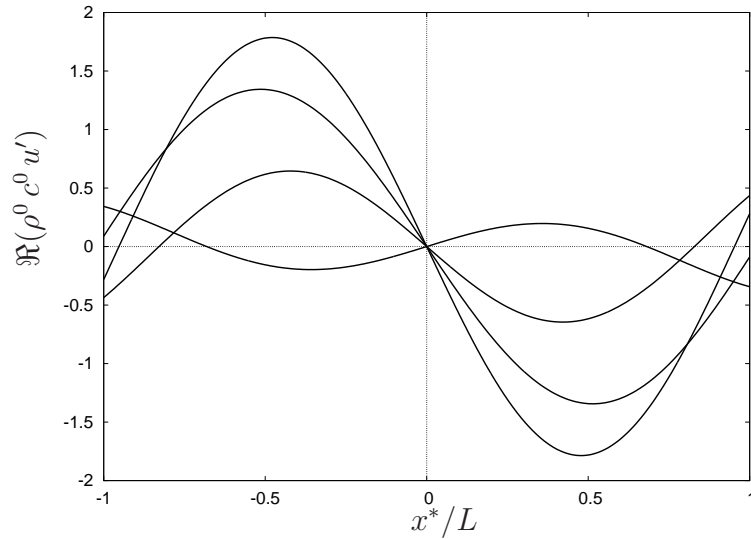


Figure A.26: $N = 1$ - Snapshots of the velocity fluctuation at different instants for the first mode ($p = 1$) and $\epsilon_1 = 0.1 + 0.2j$. A^+ was set to 1. The injector is positioned at $x^*/L \pm 1$.

References

- [1] W. Krebs, P. Flohr, B. Prade, S. Hoffmann, *Combust. Sci. Tech.* 174 (2002) 99–128.
- [2] B. Schuermans, V. Bellucci, C. O. Paschereit, *ASME Conference Proceedings 2003* (2003) 509–519.
- [3] T. Lieuwen, V. Yang, *Combustion instabilities in gas turbine engines: operational experience, fundamental mechanisms and modeling*, American Institute of Aeronautics and Astronautics, 2005.
- [4] A. P. Dowling, *J. Sound Vib.* 180 (1995) 557–581.
- [5] M. Lohrmann, H. Buchner, N. Zarzalis, W. Krebs, *ASME Conference Proceedings 2003* (2003) 109–118.
- [6] G. Staffelbach, L. Gicquel, G. Boudier, T. Poinsot, *Proc. Combust. Inst.* 32 (2009) 2909–2916.
- [7] T. Poinsot, A. Trouvé, D. Veynante, S. Candel, E. Esposito, *J. Fluid Mech.* 177 (1987) 265–292.

- [8] T. Lieuwen, B. T. Zinn, *Proc. Combust. Inst.* 27 (1998) 1809–1816.
- [9] A. Giauque, L. Selle, T. Poinso, H. Buechner, P. Kaufmann, W. Krebs, *J. Turb.* 6 (2005) 1–20.
- [10] J. O’Connor, S. Natarajan, M. Malanoski, T. Lieuwen, in: A. GT2010-22133 (Ed.), ASME Turbo Expo 2010, Glasgow.
- [11] D. G. Crighton, A. P. Dowling, J. E. F. Williams, M. Heckl, F. Leppington, *Modern methods in analytical acoustics, Lecture Notes*, Springer Verlag, New-York, 1992.
- [12] T. Poinso, D. Veynante, *Theoretical and Numerical Combustion*, R.T. Edwards, 2nd edition, 2005.
- [13] S. Candel, D. Durox, S. Ducruix, A. Birbaud, N. Noiray, T. Schuller, *Int. J. Acoust.* 8 (2009) 1–56.
- [14] N. Noiray, D. Durox, T. Schuller, S. Candel, *J. Fluid Mech.* 615 (2008) 139–167.
- [15] C. Pankiewitz, T. Sattelmayer, *ASME Journal of Engineering for Gas Turbines and Power* 125 (2003) 677–685.
- [16] F. Nicoud, L. Benoit, C. Sensiau, T. Poinso, *AIAA Journal* 45 (2007) 426–441.
- [17] P. Wolf, G. Staffelbach, R. Balakrishnan, A. Roux, T. Poinso, in: *Proceedings of the Summer Program, Center for Turbulence Research, NASA AMES, Stanford University, USA*, pp. 259–269.
- [18] S. R. Stow, A. P. Dowling, in: *ASME Paper, New Orleans, Louisiana*, p. 0037.
- [19] B. Schuermans, C. Paschereit, P. Monkiewitz, in: *44th AIAA Aerospace Sciences Meeting and Exhibit, volume AIAA paper 2006-0549*.
- [20] C. Sensiau, *Simulations numériques des instabilités thermoacoustiques dans les chambres de combustion aéronautiques - TH/CFD/08/127*, Ph.D. thesis, Université de Montpellier II, - Institut de Mathématiques et de Modélisation de Montpellier, France, 2008.

- [21] N. Noiray, M. Bothien, B. Schuermans, in: n3l - Int'l Summer School and Workshop on Non-normal and non linear effects in aero and thermoacoustics.
- [22] J. Moeck, M. Paul, C. Paschereit, in: ASME Turbo Expo 2010 GT2010-23577.
- [23] P. Moin, S. V. Apte, AIAA Journal 44 (2006) 698–708.
- [24] K. Mahesh, G. Constantinescu, S. Apte, G. Iaccarino, F. Ham, P. Moin, in: ASME J. Appl. Mech. , volume 73, pp. 374–381.
- [25] P. Schmitt, T. Poinsot, B. Schuermans, K. P. Geigle, J. Fluid Mech. 570 (2007) 17–46.
- [26] L. Selle, G. Lartigue, T. Poinsot, R. Koch, K.-U. Schildmacher, W. Krebs, B. Prade, P. Kaufmann, D. Veynante, Combust. Flame 137 (2004) 489–505.
- [27] P. Wolf, G. Staffelbach, A. Roux, L. Gicquel, T. Poinsot, V. Moureau, C. R. Acad. Sci. Mécanique 337 (2009) 385–394.
- [28] W. Lang, T. Poinsot, S. Candel, Combust. Flame 70 (1987) 281–289.
- [29] G. Bloxsidge, A. Dowling, N. Hooper, P. Langhorne, AIAA Journal 26 (1988) 783–790.
- [30] D. Bohn, E. Deuker (1993).
- [31] U. Krüger, J. Hüren, S. Hoffmann, W. Krebs, D. Bohn, ASME paper (1999) 111.
- [32] U. Kruger, J. Huren, S. Hoffmann, W. Krebs, P. Flohr, D. Bohn, Journal of Engineering for Gas Turbines and Power 123 (2001) 557–566.
- [33] S. Evesque, W. Polifke, ASME Conference Proceedings 2002 (2002) 321–331.
- [34] M. Fleifil, A. Annaswamy, Z. Ghoneim, A. Ghoniem, Combustion and Flame 106 (1996) 487–510.
- [35] L. Crocco, J. American Rocket Society 21 (1951) 163–178.

- [36] S. Evesque, W. Polifke, C. Pankiewitz, in: 9th AIAA/CEAS Aeroacoustics Conference, volume AIAA paper 2003-3182.
- [37] A. Kaufmann, F. Nicoud, T. Poinsot, *Combust. Flame* 131 (2002) 371–385.
- [38] G. Boudier, L. Y. M. Gicquel, T. Poinsot, D. Bissières, C. Bérat, *Combust. Flame* 155 (2008) 196–214.
- [39] M. S. Howe, *Proc. R. Soc. Lond. A*, Mathematical and Physical Sciences 366 (1979) 205–223.
- [40] E. Gullaud, S. Mendez, C. Sensiau, F. Nicoud, T. Poinsot, *C. R. Acad. Sci. Mécanique* 337 (2009) 406–414.